Three-Dimensional Asymmetric Flow and Temperature Fields in Cracking Furnaces†

Arno J. M. Oprins, Geraldine J. Heynderickx,* and Guy B. Marin

Laboratorium voor Petrochemische Techniek, Krijgslaan 281(S5), B9000 Gent, Belgium

Three-dimensional flue gas flow fields and temperature profiles are calculated in a 4/2/1 split coil naphtha-cracking furnace with long flame burners and an asymmetric flue gas outlet. The heat streams in the furnace connected to the asymmetric flue gas flow fields are found to be compensated for by a net radiative heat transfer in the opposite direction. As a result, the temperature distribution in the furnace remains nearly symmetrical. A furnace simulation under conditions of nonuniform heating confirms the compensating nature of radiative heat streams in the furnace. Furthermore, nonuniform heating was found to improve the thermal efficiency of the furnace and the cracking results. Optimization of heating conditions remains a point of interest.

Introduction

Thermal cracking of hydrocarbons is an endothermal process that takes place in tubular reactor coils suspended in large gas-fired furnaces. Heat transfer to the reactor tubes is mainly due to radiation from the furnace refractory walls at temperatures up to 1500 K and to radiation from the flue gas with temperatures up to 2100 K. In general, the fuel gas, burned in long flame burners in the bottom of the furnace or in radiation burners in the side walls of the furnace, is equally distributed over all burners in the furnace. Simulations of a furnace fired with long flame burners and with the flue gas outlet in the furnace side wall near the top of the furnace have shown that there is a highly asymmetric flue gas flow through the furnace.[1] The flue gas flow at the side of the reactor tube row where the flue gas outlet is located is considerably higher than the flue gas flow at the other side of the reactor tube row, even at a considerable distance from the outlet. The higher the position in the furnace, the stronger the difference in flue gas flow. However, this asymmetry in flue gas flow does not result in nonuniformities in temperature distribution. The heat transfer in a furnace with long flame burners and an asymmetric flue gas outlet is investigated using a reactor model,[2,3] a furnace model,[4] and a computational fluid dynamics (CFD) model[5] developed at the Laboratory for Petrochemical Engineering. Also, the effect of a nonuniform fuel gas feed to the burners on the furnace behavior and thermal efficiency is examined.

Model Equations

In the reactor model, a set of continuity equations for the process gas species is solved simultaneously with an energy and a pressure drop equation. A detailed description of the reactor model and of the reaction mechanism for the thermal cracking of hydrocarbons, containing over 1000 reactions between 128 species, is given by Heynderickx and Froment.[6] For the calculation of the radiative heat transfer, the furnace model uses the zone method of Hottel and Sarofim.[7] The furnace wall, tube skin, and flue gas volumes are divided into a number of surface and volume zones that are considered to be isothermal elements with constant properties. For each of these zones an energy balance is constructed and solved, taking into account conductive, convective, and radiative heat transfer. Detailed information on the coupled simulation of a furnace and a reactor is given by Rao et al.[4] and by Plehiers and Froment.[8]

The steady-state flue gas flow pattern calculation in the furnace is based on the Reynolds-averaged Navier−Stokes equations. The continuity, momentum, and energy equations are

$$\sum_{i=1}^{3}\frac{\partial}{\partial x_i}(\rho_g U_i) = 0 \tag{1}$$

$$\sum_{j=1}^{3}\frac{\partial}{\partial x_j}(\rho_g U_j U_i) = -\frac{\partial p}{\partial x_i} + \sum_{j=1}^{3}\frac{\partial}{\partial x_j}\left(\mu_t\left(\frac{\partial U_i}{\partial x_j} + \frac{\partial U_j}{\partial x_i}\right)\right) \tag{2}$$

$$\sum_{i=1}^{3}\frac{\partial}{\partial x_i}(\rho_g U_i(H+k+e_k)) - \sum_{i=1}^{3}\sum_{j=1}^{N}\frac{\partial}{\partial x_i}\left(\rho_g D_t \frac{\partial y_j}{\partial x_i} H_j\right) - \sum_{i=1}^{3}\frac{\partial}{\partial x_i}\left(\lambda_t \frac{\partial T}{\partial x_i}\right) = Q_{rad} \tag{3}$$

These equations are solved in an integration grid of considerably smaller volume elements than those used in the furnace radiation model. The six-flux De Marco and Lockwood[9] model is used for calculating the radiation intensity between the grid volumes. This model performs well for short-distance radiative heat transfer as encountered in the integration grid with small volumes.[5]

The $k-\epsilon$ model[10] is used for the calculation of the turbulence properties:

† Submission for the special issue of *Ind. Eng. Chem. Res.* to be published in conjunction with the United Engineering Foundation−CRE VIII conference to be held June 23−29, 2001, in Barga, Italy.

* Corresponding author. Tel.: +32.9.264.45.16. Fax: +32.9.264.49.99. E-mail: geraldine.heynderickx@rug.ac.be.

10.1021/ie0010114 CCC: $20.00
Published on Web 07/13/2001

$$\sum_{i=1}^{3}\frac{\partial}{\partial x_i}(\rho_g U_i k) = \sum_{i=1}^{3}\frac{\partial}{\partial x_i}\left(\mu_t \frac{\partial k}{\partial x_i}\right) + P_k - \rho_g \epsilon \qquad (4)$$

$$\sum_{i=1}^{3}\frac{\partial}{\partial x_i}(\rho_g U_i \epsilon) = \sum_{i=1}^{3}\frac{\partial}{\partial x_i}\left(\frac{\mu_t}{1.33}\frac{\partial \epsilon}{\partial x_i}\right) + P_\epsilon - 1.92\rho_g \frac{\epsilon^2}{k} \qquad (5)$$

The combustion is considered to be a noninstantaneous reaction with concentration profiles for fuel gas and flue gas components calculated from the Reynolds-averaged continuity equations:

$$\sum_{i=1}^{3}\frac{\partial}{\partial x_i}(\rho_g U_i y_j) = \sum_{i=1}^{3}\frac{\partial}{\partial x_i}\left(\rho_g D_t \frac{\partial y_j}{\partial x_i}\right) + R_j M_j \qquad (6)$$

Use is made of a five-step mechanism and its corresponding kinetics to describe the combustion of the fuel gas.[11]

More detailed information on the CFD model is given by Detemmerman and Froment[5] and by Heynderickx et al.[1]

Boundary Conditions and Calculation of the Flue Gas Flow Pattern

All variables except the pressure are prescribed at the inlet of the furnace. At the furnace outlet, the pressure is imposed. Wall functions are used to bridge the laminar boundary layer near tube and reactor walls, thus replacing the $k-\epsilon$ model.

The integration of the CFD model uses a finite volume technique. The convective terms are treated according to a first-order flux difference splitting scheme. For the viscous parts of the equations, a central difference scheme is used. The set of equations in each volume is solved using Gauss elimination. More detailed information is given by De Saegher et al.[12] and by Heynderickx et al.[1] A global flowchart of the calculations is given in Figure 1.

Furnace Description and Operating Conditions

The main dimensions and operating conditions of the simulated furnace are summarized in Table 1. Four reactors of the 4/2/1 split type (i.e., four inlets and one outlet for each coil) are suspended in the furnace. The process gas makes six passes through the furnace. A front and top view of the furnace are shown in Figure 2. The different passes of the reactor coil through the furnace have different diameters due to the split coil concept with changing process gas flows. The composition of the naphtha cracked in these coils is summarized in Table 1. For the reactor calculations, a feed of 8 different paraffins, 29 isoparaffins, 21 naphthenes, and 5 aromatics is taken into account.

The furnace is heated by means of 20 long flame burners in the furnace floor. The position of the burners is indicated in Figure 2. The fuel gas composition is given in Table 1.

For the coupled simulation of furnace and reactor coils, the furnace is divided into 36 isothermal zones by means of 8 planes parallel to the furnace bottom and 3 planes parallel to the long furnace walls, as presented in Figure 3. For reasons of symmetry, only two reactor coils have to be simulated. To investigate the effect of the difference in flue gas flow at both sides of the reactor tube row, each zone on each tube is divided into two

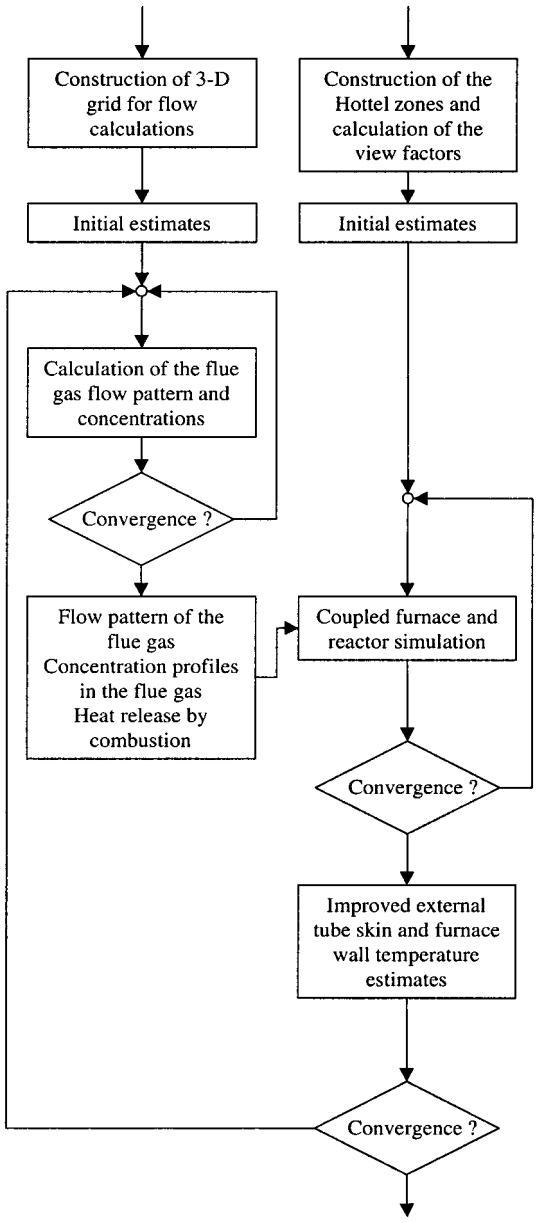

Figure 1. Global flowchart of the calculations.[4]

subzones: one zone (rear side) facing the furnace half with the flue gas outlet and one zone (front side) facing the furnace half without the flue gas outlet, resulting in a total of 480 reactor tube zones and 62 furnace wall zones. In the calculations, the flue gas is assumed to leave the furnace through an opening over the entire length of the long furnace wall.

For the calculation of the flue gas flow pattern, the bottom of the furnace is divided into 927 surface elements, as shown in Figure 3. Reactor tubes and burner openings can easily be defined in the constructed grid. The furnace is divided by means of 51 planes parallel to the furnace bottom, resulting in an integration grid with a total of 48 204 integration volumes, which was found to be adequate for a calculation of the flow pattern in combination with the coupled simulation of furnace and reactor coils.

Two simulations were performed. In a first simulation (case 1: uniform heating), the total amount of fuel gas was equally divided over the burners in the furnace. In a second simulation (case 2: nonuniform heating), the amount of fuel gas directed to the burners in the furnace

Table 1. Furnace Dimensions and Operating Conditions

Furnace	
height (m)	8
length (m)	12
width (m)	3
thickness of refractory (m)	0.16
thickness of insulation (m)	0.075
no. of burners	20
Reactor Coils	
no. of reactors	4
reactor type	4/2/1 split
no. of passes	coil
external tube diameter (10^{-2} m)	2/1/3
internal tube diameter (10^{-2} m)	8/12/16
	7/10/15
Firing Conditions	
fuel gas (tons/h)	1.5
oxygen excess (%)	1.5
fuel gas composition (wt %)	
hydrogen	5.5
methane	85.3
ethane	2.2
propane	1.2
$CO + CO_2$	1.3
total heat input (MW)	22.5
Reactor Operating Conditions	
feedstock	naphtha
feedstock composition (wt %)	
paraffins (8 components)	39.2
isoparaffins (29 components)	36.9
naphthenes (21 components)	18.5
aromatics (5 components)	5.4
feedstock feed rate (kg/h) (four coils)	11 800
steam dilution (kg/kg)	0.5
coil inlet temperature (K)	823
coil outlet pressure (atm)	1.75

half where the flue gas outlet is situated is only half the value of the amount of fuel gas directed to the burners in the other furnace half. The total amount of fuel gas, i.e., the total heat input in the furnace, remains unchanged. These operating conditions are imposed to examine the influence of nonuniform heating of the furnace on flow field, temperature profiles, heat transfer, and furnace performance.

Results and Discussion

The results of the simulations are presented in Tables 2−4 and in Figures 4−8.

Figures 4 and 5 present the calculated flue gas velocity vectors projected on a vertical and horizontal furnace cross section for simulation cases 1 (uniform heating) and 2 (nonuniform heating). For simulation case 1, with an equal distribution of the fuel gas over all burners, an asymmetric profile is obtained when the flue gas velocity vectors are projected on a vertical cross section of the furnace (Figure 4a). At a height of 4 m, 60% of the flue gas flows in the furnace half with the flue gas outlet. Near the flue gas outlet, this value has increased to 85%. The flue gas velocity vectors projected on the horizontal cross section (Figure 5a) show that the flue gas has a tendency to move around the reactor tubes and pass from one furnace half to the other by flowing between the short furnace wall and the first reactor tube. For simulation case 2, with the unequal distribution of the fuel gas over all burners, the calculated flow profile changes notably. At a height of 4 m, 50% of the flue gas flows in the furnace half with the flue gas outlet (Figure 4b). Near the flue gas outlet, this value has increased to 80%.

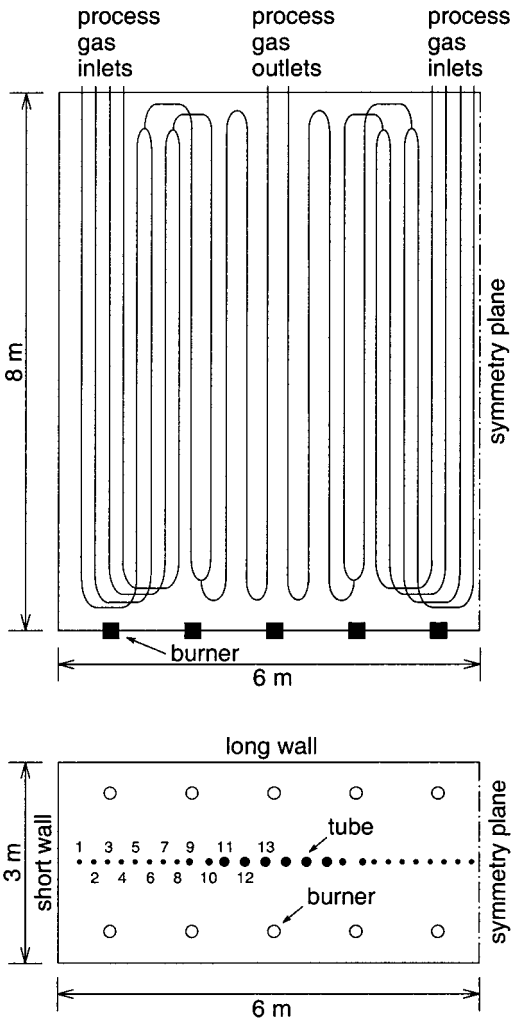

Figure 2. Naphtha cracking furnace: front and top views.

Simulation Case 1: Uniform Heating. Figure 6a presents the furnace wall and flue gas temperature profiles over the furnace height. Six curves are presented: two curves for the long furnace walls A and C (see Figure 3) and four curves for the flue gas, corresponding to four columns of nine flue gas volumes in the furnace (see Figure 3). The differences in furnace wall temperatures are negligible. The temperature of the flue gas in the outer gas columns 1 and 4 (see Figure 3) where the burners (heat sources) are located is considerably higher than the flue gas temperature in the inner columns 2 and 3, near the cracking tubes (heat sinks). The flue gas temperature variations in both furnace halves are comparable up to about 3.5 m, corresponding more or less to the height of flames. The effect of the asymmetric flue gas flow in the top part of the furnace is reflected in a difference in temperature drop for the flue gas columns near the long furnace walls. However, these temperature differences between the furnace half with the flue gas outlet and the other furnace half are small. The nearly symmetric flue gas and furnace wall temperature distribution is also reflected in the tube wall temperatures and in the heat fluxes to the tubes (not shown): the values for the front and rear sides of the tubes are almost identical. Taking into consideration that the heat fluxes to the front and rear sides of the tubes are nearly equal although there is a substantial difference in flue gas flow in both

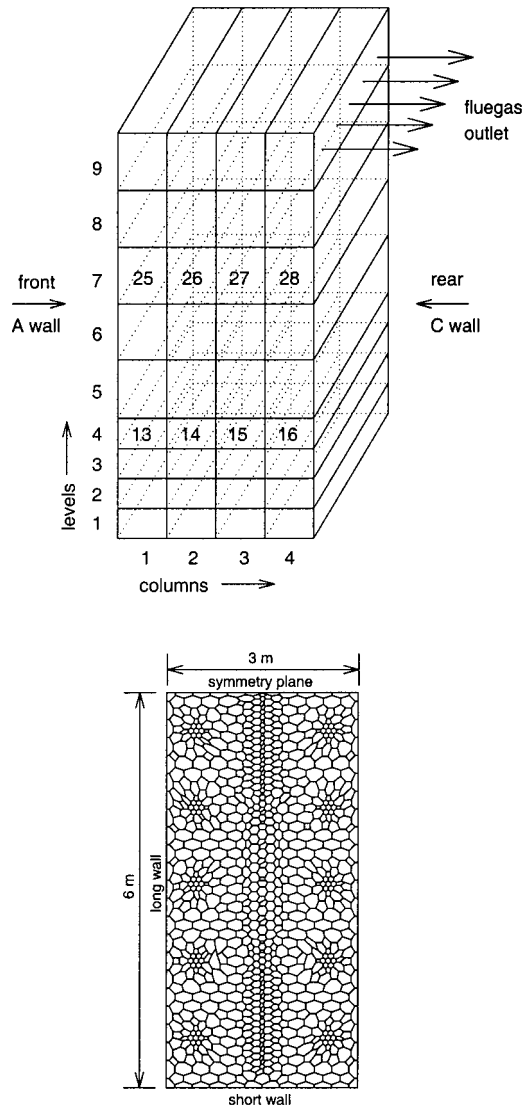

Figure 3. Hottel zones and flow calculation grid (horizontal cross section).

furnace halves, especially in the top of the furnace, the small differences in flue gas temperature in both furnace halves are rather unexpected.

To have a clear overview of the heat transport in the furnace, the energy balances for a number of representative flue gas volumes are examined more closely.

The contributions to the energy balances for the gas zones 13−16 (at furnace level 4, i.e., at the top of the flames; see Figure 3) and for the gas zones 25−28 (at furnace level 7; see Figure 3) are constructed in Table 2. The different contributions to the energy balances are the combustion heat released in the gas zone, the convective heat, the net radiative heat transfer, and the flue gas enthalpy flows in and out of the gas zone. It is found from Table 2a that there are no considerable differences between corresponding contributions to the energy balances at furnace level 4 for gas zones 13 and 16. The same is true for gas zones 14 and 15 in the center of the furnace.

At furnace level 7, there are again no differences in the comparable energy balance contributions for the gas zones 26 and 27 in the center of the furnace. However, for gas zones 25 and 28 situated near the furnace walls, the energy balance contributions differ strongly. The net

Table 2. Contributions to the Energy Balance (Units: W) for Simulation Case 1[a]

a. Gas Zones 13−16 (Figure 3)

	gas zone			
	13	14	15	16
combustion heat	86 563	0	0	96 757
convective heat transfer	−107 484	−52 169	−44 132	−112 771
flue gas flow	566 713	230 961	197 289	595 139
radiative heat transfer	−545 582	−178 553	−155 789	−579 755
net exchange with				
reactor tubes	−253 119	−5 243	−6 411	−263 104
furnace walls	−232 685	−158 872	−142 694	−249 816
gas zones	−59 778	−14 438	−6 684	−66 835

b. Gas Zones 25−28 (Figure 3)

	gas zone			
	25	26	27	28
combustion heat	0	0	0	0
convective heat transfer	−77 190	−59 018	−60 671	−104 723
flue gas flow	216 219	145 111	150 752	390 846
radiative heat transfer	−139 465	−86 093	−90 081	−286 540
net exchange with				
reactor tubes	−178 919	55 567	53 339	−225 079
furnace walls	16 182	−140 328	−143 877	−55 732
gas zones	23 272	−1 332	585	−5 696

[a] Positive entries indicate a net heat flux directed toward the gas volume.

Table 3. Contributions to the Energy Balance (Units: W) for Simulation Case 2[a]

a. Gas Zones 13−16 (Figure 3)

	gas zone			
	13	14	15	16
combustion heat	170 310	17 582	23 844	63 478
convective heat transfer	−121 731	−62 046	−45 643	−84 565
flue gas flow	603 655	299 972	163 442	389 909
radiative heat transfer	−652 814	−255 528	−141 594	−369 223
net exchange with				
reactor tubes	−285 559	−27 380	7 337	−200 567
furnace walls	−290 359	−198 252	−139 974	−139 753
gas zones	−76 896	−29 896	−8 958	−28 904

b. Gas Zones 25−28 (Figure 3)

	gas zone			
	25	26	27	28
combustion heat	0	0	0	0
convective heat transfer	−94 566	−69 488	−66 011	−81 095
flue gas flow	324 620	210 757	187 762	236 439
radiative heat transfer	−230 755	−141 282	−121 753	−156 105
net exchange with				
reactor tubes	−210 303	40 032	43 801	−187 561
furnace walls	−31 344	−171 156	−156 927	10 331
gas zones	10 891	−10 158	−8 627	21 124

[a] Positive entries indicate a net heat flux directed toward the gas volume.

amount of heat radiated by gas zone 25 (i.e., in the furnace half with the low flue gas flow) is less than half the value of the net energy radiated by gas zone 28 (i.e., in the furnace half with the high flue gas flow). The net amount of energy radiated by the gas zones is further divided into three contributions: net exchange with reactor tubes, furnace walls, and gas volumes. If these contributions are compared for gas zones 25 and 28, it is found that gas zone 25 (i.e., in the furnace half with low flue gas flow) receives net radiative energy from the furnace wall and the gas zones, while gas zone 28 (i.e., in the furnace half with high flue gas flow) emits net radiative energy to the furnace walls and the gas zones. This is also found from Figure 7a in which each point presents the net radiative heat exchange between a gas

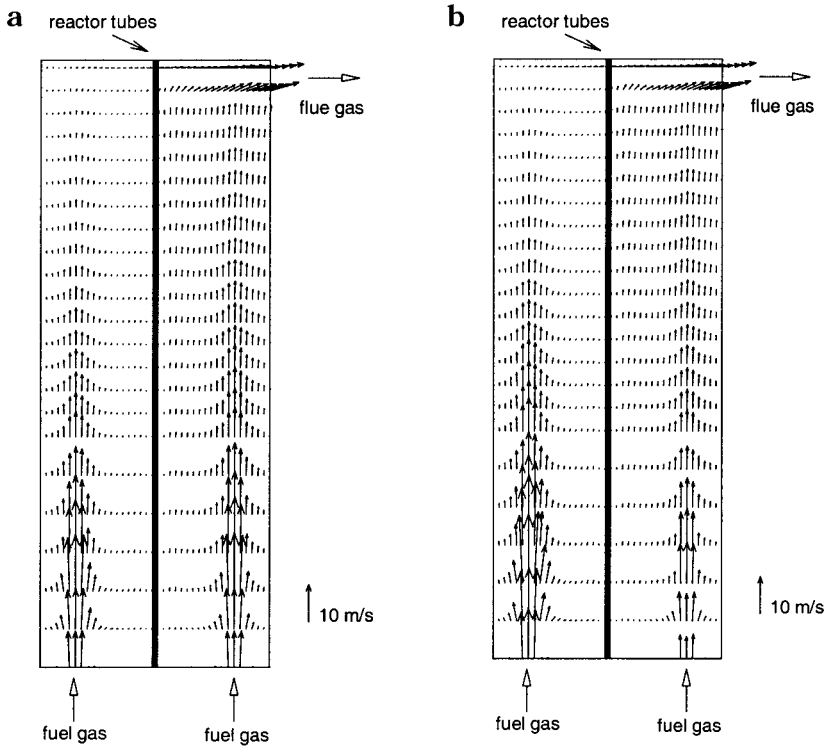

Figure 4. Flue gas velocity vector profiles projected on a vertical cross section. (a) Simulation case 1: uniform heating. (b) Simulation case 2: nonuniform heating.

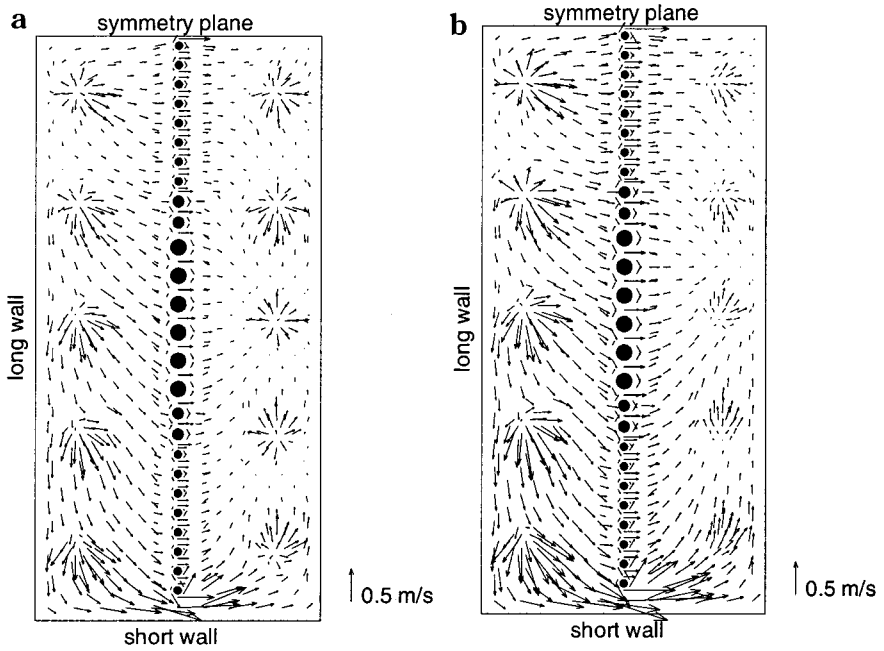

Figure 5. Flue gas velocity vector profiles projected on a horizontal cross section (at 1.52 m). (a) Simulation case 1: uniform heating. (b) Simulation case 2: nonuniform heating.

zone and all other gas zones. Four curves, one for each vertical column of nine gas zones, are shown. It is seen that, from furnace level 6 on, the gas zones in the furnace half with the low flue gas flow (column 1) receive radiative heat from the other gas zones, while the gas zones in the furnace half with the high flue gas flow (column 4) emit radiation toward the other gas zones up to level 8. Comparable results are found if the net radiative heat exchange between a gas zone and the furnace walls is shown.

Because of the asymmetric radiative heat transfer in the furnace, the flue gas temperature distribution in both furnace halves remains more or less symmetrical. The heat streams in the furnace connected to the flue gas flow directed toward the furnace half where the flue gas outlet is situated are *compensated* for by a net radiative heat transfer in the opposite direction, thus retaining temperature and heat flux symmetry in the furnace with respect to the tube row.

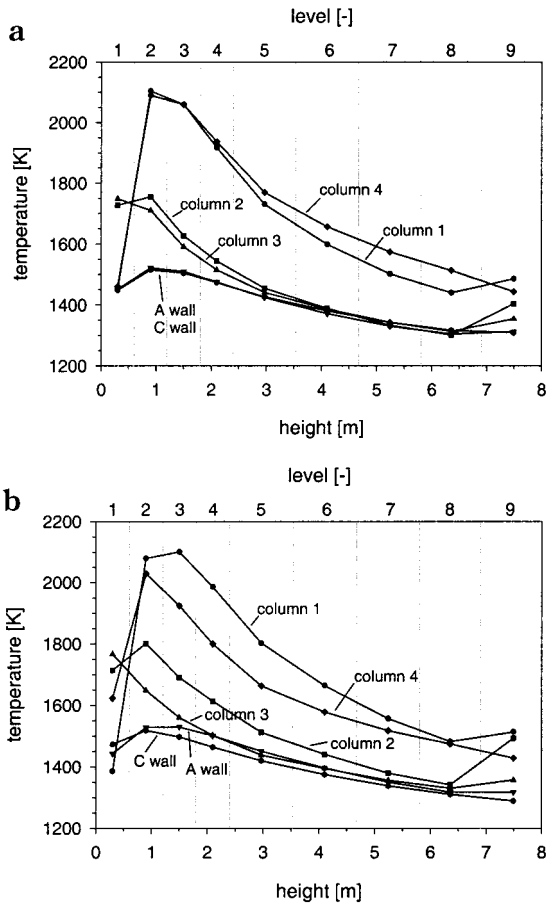

Figure 6. Long furnace wall and gas temperature profiles. (a) Simulation case 1: uniform heating. (b) Simulation case 2: nonuniform heating.

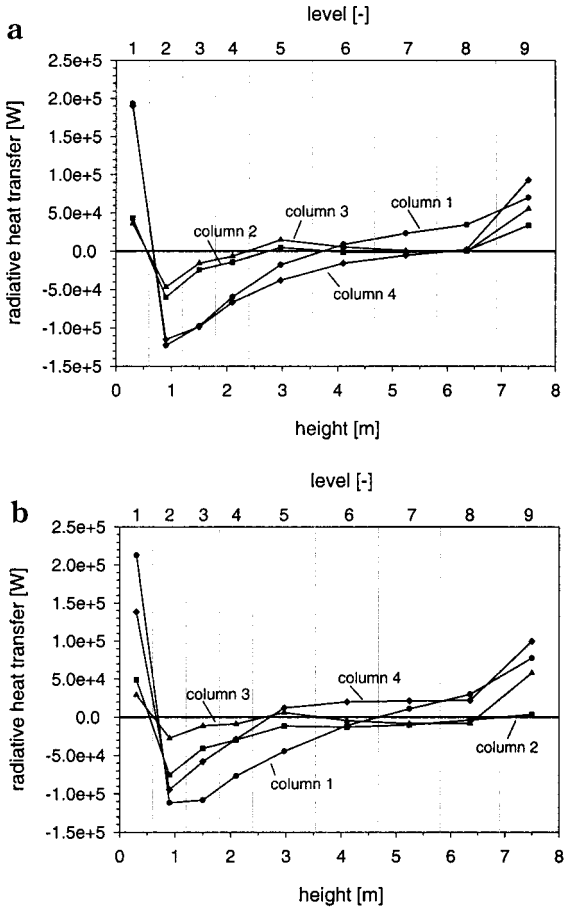

Figure 7. Net radiative heat transfer between gas zones. (a) Simulation case 1: uniform heating. (b) Simulation case 2: nonuniform heating.

Table 4. Simulation Results

	case 1	case 2
Coupled Simulation		
flue gas outlet temperature (K)	1442	1427
furnace efficiency (%)	45.4	46.1
maximum heat flux (kW/m^2)	132	131
coil outlet temperature (K)	1108	1114
max tube skin temperature (K)	1310	1311
naphtha conversion (%)	92.8	93.7
ethylene yield (wt %)	27.3	27.7
propylene yield (wt %)	16.1	15.9
max coking rate (kg/m^2 s)	1.45×10^{-6}	1.42×10^{-6}
Flow Pattern Calculation		
max flue gas velocity (m/s)	16	20
flue gas outlet velocity (m/s)	7	7
max flame temperature (K)	2100	2100

A possible consequence of the specific flue gas flow, oriented toward the asymmetrically positioned flue gas outlet, is a nonoptimal use of the heat input in the furnace, as the flue gas is pushed toward the furnace wall in which the flue gas outlet is situated (Figure 3). To examine this, a drastic change in the fuel gas distribution over the burners was imposed. The amount of fuel gas directed to the burners in the furnace half with the flue gas outlet is changed to half the value of that in the other furnace half. The total input heat input remains unchanged.

Simulation Case 2: Nonuniform Heating. The calculated flue gas velocity vectors are shown in Figures 4b and 5b. The calculated furnace wall and flue gas temperature profiles are shown in Figure 6b. The temperature distribution in the furnace is no longer nearly symmetrical with respect to the tube row as in case 1. This is due to the large differences in heat input through the burners in both furnace halves. A study of

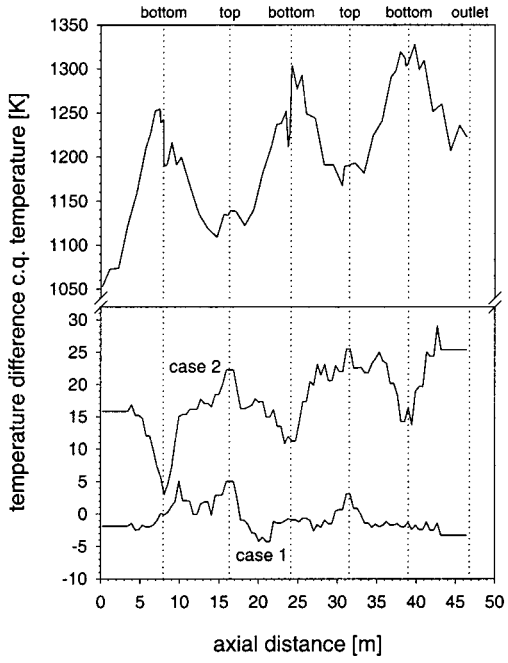

Figure 8. Typical tube skin temperature profile along the coil (top) and temparature differences between the front and rear sides of the reactor tubes for simulation cases 1 and 2 (bottom).

the energy balances in the furnace (Table 3) shows that there are no more symmetries in the energy balance contributions for corresponding gas zones. The net amount of energy radiated by gas zones 13 (i.e., in the furnace half with the high fuel gas input; see Table 3a) is considerably higher than that of gas zone 16 (i.e., in the furnace half with the low fuel gas input). Again, a *compensating* radiative heat transfer is calculated in the furnace, in this case compensating for the low heat input in the furnace half with the flue gas outlet and not compensating for heat streams due to flue gas flow from one furnace half to the other as in case 1. As a consequence the compensating radiative heat transfer in case 2 is directed in the same direction as the asymmetric flue gas flow in the furnace. However, the differences between both furnace halves due to the nonuniform fuel gas distribution are so large that they cannot be compensated for completely by radiative heat exchange. Even at level 7, where the highest flue gas flow has already shifted to the furnace half with the flue gas outlet, there is still a net radiative heat transfer toward this furnace half. These effects are readily seen in Figure 7b, where each point presents the net radiative heat exchange between a gas zone and all other gas zones. It is found that, from furnace level 5 on, the gas volumes in the furnace half with the flue gas outlet receive net radiative heat from the other gas zones, while the gas volumes in the other furnace half emit net radiative heat toward the other gas zones up to level 6.

As a consequence of the asymmetrical flue gas and furnace wall temperatures (Figure 6b), the heat fluxes to the front and rear sides of the tubes differ, resulting in differences in the tube skin temperature of front and rear tube walls. Figure 8 presents a typical tube skin temperature profile and the (smoothed) differences in the tube skin temperature between front and rear walls of a reactor tube for both simulation cases. For simulation case 1 these differences oscillate around 0 K. For simulation case 2, the asymmetric heating of the furnace results in temperature differences between front and rear tube sides oscillating around 20 K. Remark that the differences are lower when the reactor tube passes through the bottom of the furnace. This is, of course, due to the presence of the hot flames at both sides of the tubes.

Finally, in Table 4, the reactor simulation results for both simulation cases are compared. The furnace thermal efficiency rises from 45.4% to 46.1% by applying a nonuniform fuel gas distribution in the furnace. As a result, the naphtha conversion rises from 92.8% to 93.7%. The ethylene yield rises from 27.3 to 27.8 wt %. The maximum tube skin temperatures and coking rates for both simulation cases are comparable. These differences are small but, considering the industrial importance and scale of the thermal cracking process, significant.

Further calculations would be necessary to find the optimal fuel gas distribution over the furnace halves.

Conclusions

An asymmetric position of the flue gas outlet in a thermal cracking furnace causes asymmetric flue gas flow profiles in the furnace. However, the heat streams in the furnace, connected to the flue gas flow toward the furnace section with the flue gas outlet, are compensated for by a net radiative heat transfer in the opposite direction. As a result, the temperature distribution in the furnace remains nearly symmetrical. A simulation of the furnace under conditions of nonuniform heating confirms the compensating nature of radiative heat streams in the furnace. Even more, it was found that nonuniform heating can improve the thermal efficiency, and therefore the cracking results in a furnace with an asymmetric flue gas outlet.

Acknowledgment

G.J.H. and G.B.M. are grateful to the "Fonds voor Wetenschappelijk Onderzoek-Vlaanderen" (FWO-N) for financial support of the CFD Research. A.J.M.O. is grateful to DSM for a research assistentship.

Nomenclature

D_t = total diffusivity ($D_m + D_{turb}$) (m^2/s)
e_k = specific kinetic energy (J/kg)
F_j = molar flow rate of species j (mol/s)
H = enthalpy (J/kg)
H_j = enthalpy of formation for component j (J/kg)
k = turbulent kinetic energy (J/kg)
M_j = molecular weight of component j (kg/mol)
P_k = production of turbulent energy (W/m^3)
P_ϵ = dissipation of turbulent energy equation source term (J/m^3 s^2)
p = total pressure (Pa)
Q_{rad} = net radiative heat exhange (W/m^3)
R_j = rate of formation of component j (mol/m^3 s)
T = temperature (K)
U_i = velocity component in the ith direction (m/s)
x_i = coordinate in the ith direction (m)
y_j = weight fraction of component j

Greek Letters

ρ_g = gas density (kg/m^3)
λ_t = total conductivity ($\lambda_m + \lambda_{turb}$) (W/m K)
μ_t = total viscosity ($\mu_m + \mu_{turb}$) (Pa s)
ϵ = dissipation of turbulent kinetic energy (m^2/s^3)

Literature Cited

(1) Heynderickx, G. J.; Oprins, A. J. M.; Dick, E.; Marin, G. B. Three-Dimensional Flow Patterns in Cracking Furnaces with Long-Flame Burners. *AIChE J.* **2001**, in press.

(2) (a) Willems, P.; Froment, G. F. Kinetic Modeling of the Thermal Cracking of Hydrocarbons, Part 1: Calculation of the Frequency Factors. *Ind. Eng. Chem. Res.* **1988**, *27*, 1959. (b) Willems, P.; Froment, G. F. Kinetic Modeling of the Thermal Cracking of Hydrocarbons, Part 2: Calculation of Activation Energy. *Ind. Eng. Chem. Res.* **1988**, *27*, 1966.

(3) Froment, G. F.; Bischoff, K. B. *Chemical Reactor Analysis and Design*; John Wiley and Sons: New York, 1990.

(4) Rao, M. V. R.; Plehiers, P. M.; Froment, G. F. Simulation of the Run Length of an Ethane Cracking Furnace. *Ind. Eng. Chem. Sci.* **1988**, *43*, 1223.

(5) Detemmerman, T.; Froment, G. F. Three-Dimensional Coupled Simulation of Furnaces and Reactor Tubes for the Thermal Cracking of Hydrocarbons. *Rev. Inst. Fr. Pét.* **1998**, *53*, 181.

(6) Heynderickx, G. J.; Froment, G. F. A Pyrolysis Furnace with Reactor Tubes of Elliptical Cross Section. *Ind. Eng. Chem. Res.* **1996**, *35*, 2183.

(7) Hottel, H. C.; Sarofim, A. F. *Radiative Heat Transfer*; McGraw-Hill: New York, 1967.

(8) Plehiers, P. M.; Froment, G. F. Firebox Simulation of Olefin Units. *Chem. Eng. Commun.* **1989**, *80*, 81.

(9) De Marco, A. G.; Lockwood, F. C. A New Flux Model for the Calculation of Radiation in Furnaces. *Riv. Combust.* **1975**, *29*, 184.

(10) Jones, W. P.; Launder, B. E. The prediction of Laminarization with a Two-Equation Model of Turbulence. *AIAA J.* **1972**, *15*, 301.

(11) Westbrook, C. K.; Dryer, F. L. Simplified Reaction Mechanisms for the Oxidation of Hydrocarbon Fuel in Flames. *Combust. Sci. Technol.* **1981**, *27*, 31.

(12) De Saegher, J. J.; Detemmerman, T.; Froment, G. F. Three-Dimensional Simulation of High-Severity Internally Finned Cracking Coils for Olefins Production. *Rev. Inst. Fr. Pét.* **1996**, *51*, 245.

Received for review November 30, 2000
Revised manuscript received April 23, 2001
Accepted May 9, 2001

IE0010114